J. Fluid Mech. (1989), *vol.* 201, *pp.* 259–278
Printed in Great Britain

Potential flow about two counter-rotating vortices approaching a free surface

By JOHN G. TELSTE
David Taylor Research Center, Bethesda, MD 20084-5000, USA

(Received 24 February 1987 and in revised form 6 September 1988)

The problem of calculating nonlinear two-dimensional free-surface potential flow about a pair of counter-rotating point vortices rising under their own influence towards a free surface is solved numerically. The two vortices are inserted into fluid which is initially at rest. A boundary/integral-equation method is used to obtain free-surface elevations and streamlines about the rising pair of vortices for several vortex strengths. The paths of the two vortices are compared with those of a counter-rotating vortex pair under a rigid wall.

1. Introduction

In recent years there has been increased interest in the interaction of underwater vortices with a free surface. Such an interaction occurs behind a hydrofoil moving under a free surface or behind a ship whose counter-rotating propellers produce the vortex flow. Numerical work on the two-dimensional interaction of a free surface with point vortices has been performed by Salvesen & von Kerczek (1976), but they considered the flow resulting from a single vortex held fixed in a uniform stream. Such a model is more appropriate for the bound vortex of a moving body than for the free vortices of interest here. Other interest is exemplified in the papers of Barker & Crow (1977), Saffman (1979) and Peace & Riley (1983), which all discuss a rebound phenomenon possessed by the vortices and determine that it is a viscous effect. Novikov (1981) has done a linear analysis of the generation of surface waves by discrete vortices in air and water. He assumed that the fluid flow is potential except at the locations of discrete vortices. Sarpkaya & Henderson (1984) reported on experimental and theoretical investigations of the underwater vortices trailing behind a hydrofoil and concluded from experiments that, after two counter-rotating underwater vortices are produced, two kinds of disturbances appear on the free surface as the vortices rise towards the water surface. One set of disturbances, which they call striations, is essentially a set of three-dimensional disturbances on the free surface that are perpendicular to the direction of motion of the foil and appear when the two vortices are at a distance from the free surface approximately equal to the initial separation between the vortices. The other disturbances, called scars, appear on the free surface at a time when the two counter-rotating vortices are within half of the initial separation distance from the surface. Scars are free-surface depressions that are more or less parallel to the direction of motion of the foil. They are essentially two-dimensional and move outward with the vortices created by the movement of the foil. In the theoretical part of their investigation of the interaction of the vortex pair behind a moving foil with a free surface, Sarpkaya & Henderson replaced the free surface by a rigid wall and assumed the flow to be two-dimensional. The vortices are treated as point vortices in two-dimensional potential flow in typical

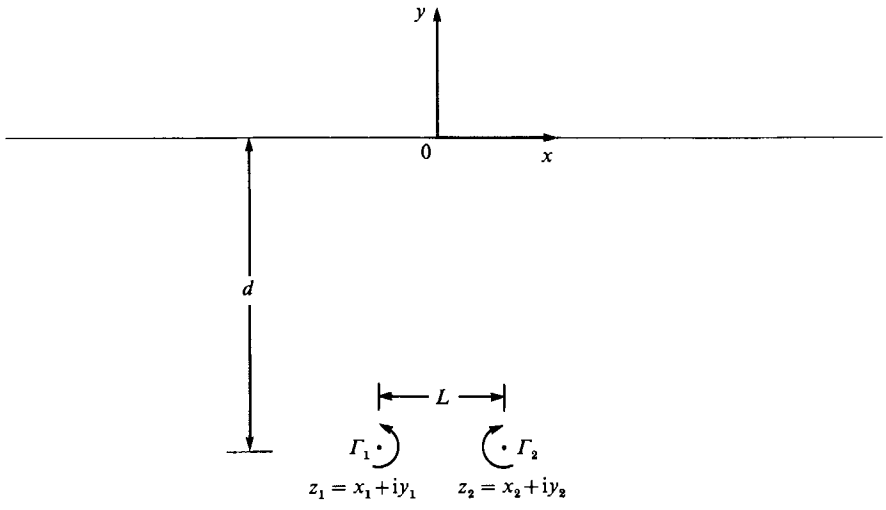

FIGURE 1. Definition sketch.

strip-theory fashion. Sarpkaya & Henderson applied the solution of Lamb (1932) to this problem of a counter-rotating vortex pair near a rigid wall.

This paper presents numerical solutions to the fully nonlinear problem of the interaction of a pair of counter-rotating vortices with a free surface. Two discrete point vortices are inserted into a fluid which is initially at rest. Except for these vortices, the motion of the fluid is assumed to be irrotational. The two counter-rotating point vortices are allowed to approach the free surface under their own influence and, in so doing, interact with the free surface. This model, of course, does not incorporate important three-dimensional phenomena such as Crow instability or other phenomena such as the flow within a finite vortex core and the decay of vorticity (Sarpkaya & Henderson). A boundary/integral-equation method is used to obtain free-surface elevations and streamlines about the rising pair of vortices for several vortex strengths. The paths of the two vortices are compared with those of a pair of counter-rotating vortices under a rigid wall.

2. Mathematical formulation

The problem considered is the calculation of two-dimensional potential flow about a pair of counter-rotating point vortices moving under their own influence towards a free surface. Each of the two point vortices has a fixed circulation. The vortex on the left has a counterclockwise circulation associated with it, and the vortex on the right has the opposite circulation. The two vortices are inserted into a fluid which is incompressible and inviscid, and which is initially at rest in a time-dependent region $\Omega(t)$ of infinite depth and lateral extent. Except for the two point vortices, the fluid motion is assumed to be irrotational. Surface tension is neglected. The line segment connecting the two vortices is initially parallel to the original undisturbed free surface and, because of symmetry, remains so. This symmetry is used to reduce many of the numerical calculations to only half of the fluid region. The computations in the other half are obtained from enforcing symmetry. A Cartesian (x, y) coordinate system is fixed so that the y-axis points vertically upward, the x-axis lies in the undisturbed free surface and the origin lies directly above the midpoint of the line segment connecting the two vortices (figure 1).

All variables have been non-dimensionalized. Lengths have been scaled by the initial distance L between the two vortices; velocities by Γ/L, where Γ is the magnitude of the circulation of the vortices; and time by L^2/Γ. The location of the free-surface boundary $\partial\Omega_F$ is unknown and must be computed as part of the solution. The locations of the discrete vortices are given by $z_1 = x_1 + iy_1$ and $z_2 = -x_1 + iy_1$ in which $x_1 < 0$. The vortex at z_1 has positive circulation while the vortex at z_2 has the opposite circulation. The assumptions guarantee the existence of a velocity potential ϕ everywhere in the fluid region except at the two discrete vortices. This potential satisfies an initial/boundary-value problem given by the following equations:

$$\phi_{xx} + \phi_{yy} = 0 \quad \text{in} \quad \Omega(t) - \{z_1, z_2\}; \tag{1}$$

$$\frac{Dx}{Dt} = \phi_x \quad \text{on} \quad \partial\Omega_F; \tag{2}$$

$$\frac{Dy}{Dt} = \phi_y \quad \text{on} \quad \partial\Omega_F; \tag{3}$$

$$\frac{D\phi}{Dt} = \tfrac{1}{2}(\phi_x^2 + \phi_y^2) - \frac{y}{F_r^2} \quad \text{on} \quad \partial\Omega_F; \tag{4}$$

$$\frac{dx_1}{dt} = \frac{\partial}{\partial x}\left(\phi - \frac{1}{2\pi}\tan^{-1}\frac{y-y_1}{x-x_1}\right) \quad \text{at} \quad (x,y) = (x_1, y_1); \tag{5}$$

$$\frac{dy_1}{dt} = \frac{\partial}{\partial y}\left(\phi - \frac{1}{2\pi}\tan^{-1}\frac{y-y_1}{x-x_1}\right) \quad \text{at} \quad (x,y) = (x_1, y_1); \tag{6}$$

$$\phi_x = 0 \quad \text{for} \quad x = \pm\infty, (x,y) \quad \text{in} \quad \Omega(t); \tag{7}$$

$$\phi_y = 0 \quad \text{for} \quad -\infty < x < \infty, \quad y = -\infty; \tag{8}$$

$$\phi(t=0) = 0 \quad \text{for} \quad (x,y) \quad \text{on} \quad \partial\Omega_F(t=0); \tag{9}$$

$$y(t=0) = 0 \quad \text{on} \quad \partial\Omega_F(t=0). \tag{10}$$

The subscripts x and y denote partial differentiation with respect to these variables, and the derivative D/Dt denotes a material derivative. The Froude number is $F_r = \Gamma/(gL^3)^{\frac{1}{2}}$. Equations (1)–(4) are well known and have been used by Longuet-Higgins & Cokelet (1976) and others. Equations (5) and (6) stem from a theorem due to Helmholtz, which states that vortex lines move with the velocity of fluid particles (Lamb 1932). The terms involving the inverse tangent function represent the potential of a point vortex. Equation (9) is consistent with equation (13.54) of Wehausen & Laitone (1960) when t is allowed to approach zero.

3. Method of solution

The initial/boundary-value problem is solved by the generalized vortex method of Baker, Meiron & Orszag (1981, 1982). In this method, the velocity potential is represented as the sum of the velocity potential due to the two discrete vortices and the velocity potential due to a distribution of vortices on the free surface. The free surface z_F and the vortex distribution γ on it are parametrized in terms of the time t and a parameter e as $z_F(e,t) = x_F(e,t) + iy_F(e,t)$ and $\gamma(e,t)$, in which $-\infty < e < \infty$

and $t \geqslant 0$. Thus the complex velocity potential $w(z) = \phi + \mathrm{i}\psi$ at $z = x + \mathrm{i}y$ in the fluid region $\Omega(t)$ is written as

$$w(z) = \frac{1}{2\pi\mathrm{i}} \int_{-\infty}^{\infty} \gamma(e') \log (z - z_{\mathrm{F}}(e'))\, \mathrm{d}e' + \frac{1}{2\pi\mathrm{i}} \log (z - z_1) - \frac{1}{2\pi\mathrm{i}} \log (z - z_2). \tag{11}$$

The velocity of a free-surface vortex at $z_{\mathrm{F}}(e,t)$, for fixed e, is defined by the equation

$$\frac{\partial z_{\mathrm{F}}^*}{\partial t}(e,t) \equiv \tilde{q}^*(e) = q^*(e) + \frac{\alpha\gamma(e)}{2(z_{\mathrm{F}}(e,t))_e}, \tag{12}$$

in which $q(e)$ is the principal-value velocity defined on the free surface and α is a constant to be discussed later. Free-surface vortices are at fixed values of e and can slide along the free surface. The asterisk denotes complex conjugation, and the subscript e denotes partial differentiation with respect to e. The velocities of the discrete vortices at z_1 and z_2 are given by (5) and (6), which can be expressed in complex-variable notation as

$$\frac{\mathrm{d}z_k}{\mathrm{d}t} = \frac{\mathrm{d}}{\mathrm{d}z}\left[w + \frac{(-1)^k}{2\pi\mathrm{i}} \log (z - z_k)\right] \quad \text{at } z = z_k \quad \text{for} \quad k = 1, 2. \tag{13}$$

Application of the dynamic free-surface boundary condition (4) to (11) leads to the evolution equation for γ:

$$\frac{\partial\gamma}{\partial t}(e) = \left(\frac{\alpha}{2} - \frac{1}{4}\right) \frac{\partial}{\partial e}\left[\frac{\gamma^2}{(z_{\mathrm{F}})_e (z_{\mathrm{F}})_e^*}\right] - 2\left\{\mathrm{Re}\left[\frac{\partial q^*}{\partial t}(z_{\mathrm{F}})_e - \frac{\alpha\gamma}{2}\frac{q_e}{(z_{\mathrm{F}})_e}\right] + \frac{(y_{\mathrm{F}})_e}{F_r^2}\right\}. \tag{14}$$

The functions q_e and $\partial q^*/\partial t$ are obtained by differentiation of $q(e)$. It is expected that (7) will be satisfied if

$$\lim_{e \to \pm\infty} \gamma(e) = 0. \tag{15}$$

The initial/boundary-value problem defined by (1)–(10) is solved if the functions z_{F} and γ along the free surface and the functions z_1 and z_2 are obtained as functions of time. These functions satisfy a system of differential evolution equations, parametrized by e, consisting of (12) for the free surface, (13) for the positions of the discrete vortices and (14) for the circulation density along the free surface. Equation (14) is a Fredholm integral equation of the second kind for $\partial\gamma/\partial t$. The corresponding initial conditions are

$$z_{\mathrm{F}}(e) = 0, \tag{16}$$

$$\gamma(e) = 0, \tag{17}$$

and

$$z_k = \frac{(-1)^k}{2} - \mathrm{i}d \quad \text{for} \quad k = 1, 2, \tag{18}$$

in which d is the initial depth of the vortex pair.

Since the free surface is infinitely long, it is necessary to introduce wave damping to reduce to a finite length the part for which computation is required. Numerical damping has been discussed by Baker *et al.* (1981) and Israeli & Orszag (1981). To introduce this damping, the free-surface vortex density and height are set to zero

outside the region $|x| < x_R$, and in the region $|x| < x_R$ the free-surface position and the vortex density along the free surface obey the modified evolution equations

$$\frac{\partial x_F}{\partial t}(e) = R_1, \tag{19}$$

$$\frac{\partial y_F}{\partial t}(e) = I_1 - D_F|(|x_F(e)| - x_D)|\, y_F(e), \tag{20}$$

and

$$\frac{\partial \gamma}{\partial t}(e) = R_2 - D_F|(|x_F(e)| - x_D)|\, \gamma_F(e). \tag{21}$$

$R_1 - iI_1$ is the right-hand side of (12), and R_2 is the right-hand side of (14). Here D_F is zero if $|x| < x_D$ and D_F is non-zero if $x_D < |x| < x_R$. Thus there is a region $|x| < x_D$ in which (19)–(21) reduce to the undamped (12) and (14), a region $x_D < |x| < x_R$ where waves entering from $|x| < x_D$ are damped, and a region $|x| > x_R$ where the water remains undisturbed. Although D_F has a finite jump along the free surface, the added terms in (20) and (21) are in fact continuous along the free surface. Computations can then be restricted to $|x| < x_R$.

The functions $z_F(e,t)$ and $\gamma(e,t)$ are discretized spatially by defining the functions

$$(z_F)_j(t) \equiv (x_F)_j(t) + i(y_F)_j(t) = z_F(e_j, t) \tag{22}$$

and

$$\gamma_j(t) = \gamma(e_j, t), \tag{23}$$

where $t \geqslant 0$ and $j = 1, 2, \ldots, N$. The initial definition of these discretized functions is given by

$$(z_F)_j(0) \equiv (x_F)_j(0) + i(y_F)_j(0) \tag{24}$$

and

$$\gamma_j(0) = 0. \tag{25}$$

The parametrization e is chosen in such a way that $e_j = j$. The number N of free-surface points used and the distribution of the points on the free surface varies with the particular problem being solved.

For each j, the functions $(z_F)_j(t)$ and $\gamma_j(t)$ obey ordinary differential equations obtained from (19)–(21) by discretizing the right-hand sides spatially. The integrals are replaced by sums based on trapezoidal quadrature, and spatial derivatives with respect to e are computed using fourth-order finite-difference formulas. Typical of this discretization is the replacement of the principal-value integral

$$\int_{-\infty}^{\infty} \frac{\gamma(e')\,de'}{z_F(e) - z_F(e')}$$

by the sum

$$\sum_{k \neq j} \frac{\gamma_k \Delta e}{(z_F)_j - (z_F)_k},$$

in which e and e' are associated with the indices j and k respectively. The ordinary differential equations for $\gamma_j(t)$ are Fredholm integral equations of the second kind for $\partial\gamma_j/\partial t$ with eigenvalues that guarantee the convergence of an iterative solution technique for the derivatives (Baker *et al.* 1982). The result of the discretization process is a coupled nonlinear system of ordinary differential equations for $(z_F)_j(t)$ and $\gamma_j(t)$. There are $3N+2$ equations in this system of equations.

The method chosen to solve the system of differential equations numerically is an implicit fourth-order Adams–Bashforth–Moulton predictor–corrector scheme. The first few time steps are treated with an explicit fourth-order Runge–Kutta technique. Numerical instabilities arise on the computed free surface if a filtering scheme is

not used. The numerical filtering scheme, which involves filtering the (x, y)-parametrization of the free surface and the vortex strength along the free surface, is employed sparingly at the beginning of the calculation and more frequently later in the calculations when the need arises. Filtering was discussed by Shapiro (1975) and has been used by Longuet-Higgins & Cokelet (1976) and Haussling & Coleman (1979) to eliminate numerical instabilities. Energy conservation can be monitored to assure that the filtering is not removing energy from the flow.

4. Results

Three cases corresponding to $1/F_r^2 = 0.02$, 0.2 and 4.0 are considered and will be referred to as cases (a), (b) and (c), respectively. These three cases fall outside the range of Froude numbers (corresponding to $1/F_r^2$ between 33 and 333) for which Sarpkaya & Henderson (1984) did their experimental and theoretical work. The circulation of the discrete vortices is greater in the three cases presented here. In each case the vortex paths are plotted with the paths the vortices would have followed had the free surface been replaced with a rigid wall. The free surface and streamlines near the vortices are provided for selected times. In addition, the potential energy (V), the negative of the finite part of the kinetic energy ($-T$) and the negative of the finite part of the total energy ($-W$) have been plotted as functions of time. These quantities are defined by (A 1), (A 3) and (A 4) of the Appendix, where the invariance of W is discussed. Hereafter, the negative of the finite part of the kinetic energy will be referred to as the kinetic energy, and the negative of the finite part of the total energy will be referred to as the energy of the fluid. In each case the initial depth of the vortex pair is 5, i.e. five times the initial distance between the vortices. This depth was chosen to be large enough to prevent significant initial transients on the free surface.

The free surface has been discretized in two ways in accordance with (22)–(25). Both discretizations are similar in that the resulting free-surface grid is uniform for $|x| < 5$ and an expanding grid, which increases by 1% from interval to interval, is created for $|x| > 5$. For cases (a) and (b), the number N of free-surface points is 641 and the uniform mesh spacing in $|x| < 5$ is 0.0625. Thus the initial free-surface grid is given by

$$(z_F)_j(t=0) = \begin{cases} -79h - 100h(1.01^{242-j} - 1) & \text{for} \quad 1 \leqslant j \leqslant 240 \\ [j - \frac{1}{2}(N+1)]\,h & \text{for} \quad 241 \leqslant j \leqslant 401 \\ 79h + 100h(1.01^{j-400} - 1) & \text{for} \quad 402 \leqslant j \leqslant 641, \end{cases} \tag{26}$$

in which h is 0.0625. The mesh extends from about -67 to about 67; in other words, $x_R = x_{641} \approx 67$. The wave damping region at either extremity includes about 40 points of the grid and has a length of 20; that is, $x_D = x_{641} - 20$. The resulting damping regions are for $|x|$ between 47 and 67. Concerns about the accuracy of the computations for case (c) led to the use of a uniform grid in $|x| < 5$ with twice as many points. This grid extends from about $x = -376$ to 376, and the wave damping region at either extremity of the computational region is 70 units in length. This second free-surface discretization is given by

$$(z_F)_j(t=0) = \begin{cases} -159h - 100h(1.01^{482-j} - 1) & \text{for} \quad 1 \leqslant j \leqslant 480 \\ [j - \frac{1}{2}(N+1)]\,h & \text{for} \quad 481 \leqslant j \leqslant 801 \\ 159h + 100h(1.01^{j-800} - 1) & \text{for} \quad 802 \leqslant j \leqslant 1281, \end{cases} \tag{27}$$

in which h is 0.031 25. The wave damping regions are so far from the origin that significant waves will not reach them during the time for which computations are performed. Thus a precise definition of D_F is not necessary. The wave damping parameter D_F in (20) and (21) was set to 2 divided by the length of the damping region in each case. This value proved successful in previous computations.

The definition of α in (12) and (14) affects the spacing between the free-surface vortices in the discretized problem, and thus a judicious value is one for which numerical error is minimal. In particular, α should be defined so that the spacing between consecutive vortices remains fine enough to resolve free-surface features and so that the spacing does not develop large gradients at some points. When α is 1, the velocity with which a surface grid point moves is the velocity of the fluid particle at that grid point. For any other value of α, the velocity is the fluid velocity plus a velocity tangential to the free surface. The kinematic and dynamic free-surface boundary conditions are satisfied, but this velocity of a grid point does not correspond to any physical fluid velocity.

At first computations were performed with α equal to 0. In the central region between the two vertical lines passing through the discrete vortices, the free-surface grid points moved outward and tended to congregate near the vertical lines. Eventually the spacing in the central region became very coarse, and the free-surface spacing near the edges of the central region came to have a large gradient. Such conditions lead to large numerical errors. The same computations were then carried out with α set to 1. In this case the free-surface markers moved with the velocity of fluid particles and moved out of the central region at an even faster rate. One should expect such behaviour since the circulation of the two discrete vortices will carry fluid near the central part of the free surface away from the centre and parallel to the free surface. Without a mechanism for introducing new free-surface vortices near the centre, the spacing in the central portion of the free surface became coarse. Numerical experiments were also performed for α equal to -1. Of the three values of α considered, the latter choice produced the most desirable free-surface spacing with respect to resolution and uniformity. This value of α at least partially counteracts the tendency of the circulation to sweep free-surface vortices out of the central region. Since α appears linearly in (12), it seems reasonable to assume that $\alpha = -1$ is the optimal value of α for $|\alpha| \leqslant 1$. Thus all the results in this paper have been computed with α set to -1.

The Fredholm integral equations of the second kind for $\partial\gamma/\partial t$, given by (14) and (21), are solved iteratively using the Neumann series. The iterative technique is considered converged when the absolute value of the difference in two successive iterates is less than 10^{-6} plus 10^{-6} times the absolute value of the latest iterate. Thus, when the iterates are small, the error criterion is essentially an absolute error criterion, and, when the iterates are large, the error criterion behaves like a relative error criterion.

Case (*a*) ($1/F_\tau^2 = 0.02$). Results from the numerical calculation of the solution in this case of strongest circulation are depicted in figures 2–5. The time-step size used to obtain these results was initially set to 0.04 based on numerical experimentation. It was kept at this value until $t = 32.0$ when it was reduced to 0.01 for the remainder of the calculation. The time step was decreased because, as the vortex pair approached the free surface with the larger time step, the iterative scheme for obtaining the rate of change of vortex strength along the free surface began to require more than ten iterations before convergence was attained. Until $t = 25.6$, the number of iterations had been four per time step. After that, the number per time

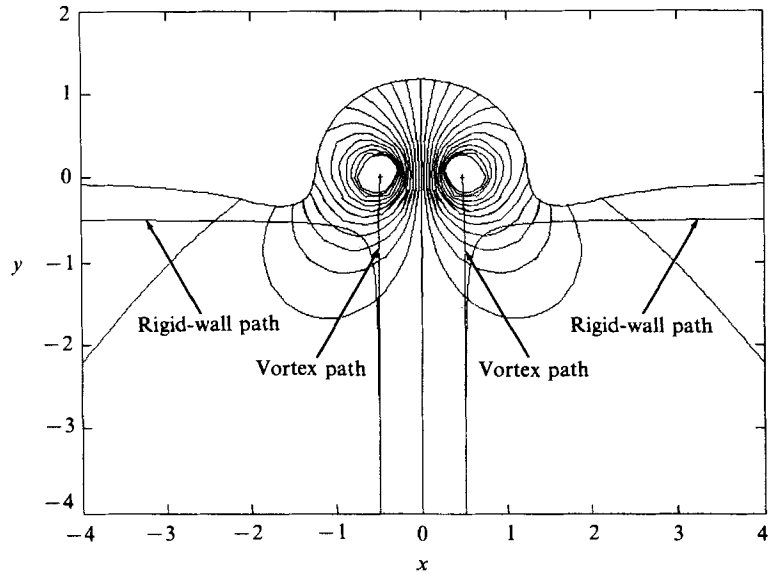

FIGURE 2. Streamlines $\psi = 0, \pm 0.02, \pm 0.04, \ldots, \pm 0.24$, vortex paths, wall paths, and the free surface for $1/F_r^2 = 0.02$ at $t = 32.0$.

step increased gradually to eleven. The rate at which the scheme converges to a solution is related to the eigenvalues of the Fredholm integral equation of the second kind for the rate of change of the vortex strength. These eigenvalues approach one as the vortex pair approaches the free surface and, as they approach one, the rate of convergence decreases (Baker *et al.* 1982). The time step was decreased so that the time derivative of the free-surface vortex strength for each time step could be obtained from that of the previous time step with fewer iterations. Even so, quartering the time-step size reduced the number of iterations by only two from eleven to nine. The number of required iterations began increasing again and, at $t = 34.0$, the number was twelve.

The linear filtering scheme was necessary but it was applied sparingly every four units of time until $t = 8.0$ and every eight units of time thereafter. The free surface, streamlines, the position of the vortex pair and the vortex paths are depicted in figures 2–4 for three times near the end of the calculation. The paths the vortex pair would follow if the free surface were replaced with a rigid wall are also depicted. In these figures, it is apparent that the circulation of each vortex is so strong that the pair moves up and away from the wall paths. In so doing, the pair produces a large free-surface displacement. Free-surface breaking will clearly occur. Figure 5 shows how the computed energy, kinetic energy and potential energy vary as functions of time. Kinetic energy of the flow is converted to potential energy of the free surface. The decrease in kinetic energy is apparent in the vortex paths being 'inside' the wall paths. The total energy $-W$ is constant throughout the calculation until near the end. The successful energy conservation throughout most of the calculation verifies that the filtering is not removing energy from the flow. The eventual loss of energy conservation may result from the distribution of grid points on the free-surface hump becoming rather coarse near the end of the calculation. The calculation was stopped at $t = 34.0$ because of the large number of iterations required to obtain solutions of the coupled integral equations, the poor free-surface resolution and the loss of energy conservation.

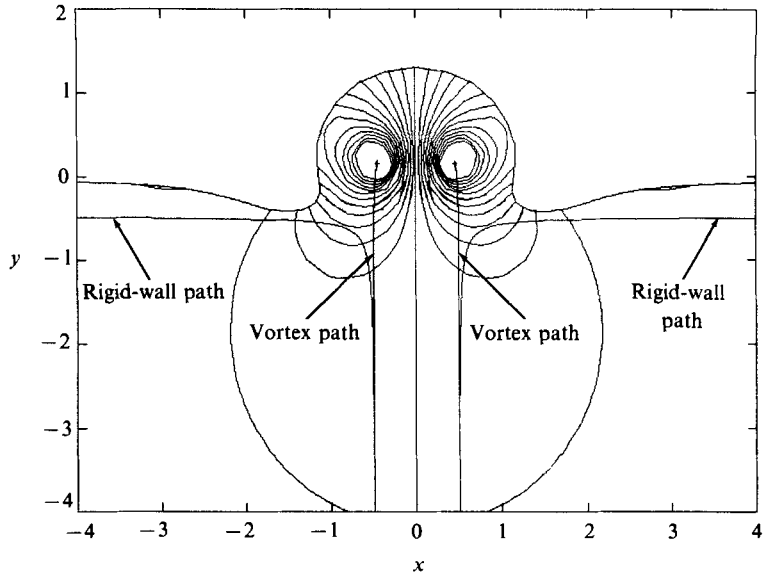

FIGURE 3. Streamlines $\psi = 0, \pm 0.02, \pm 0.04, \ldots, \pm 0.24$, vortex paths, wall paths, and the free surface for $1/F_r^2 = 0.02$ at $t = 33.0$.

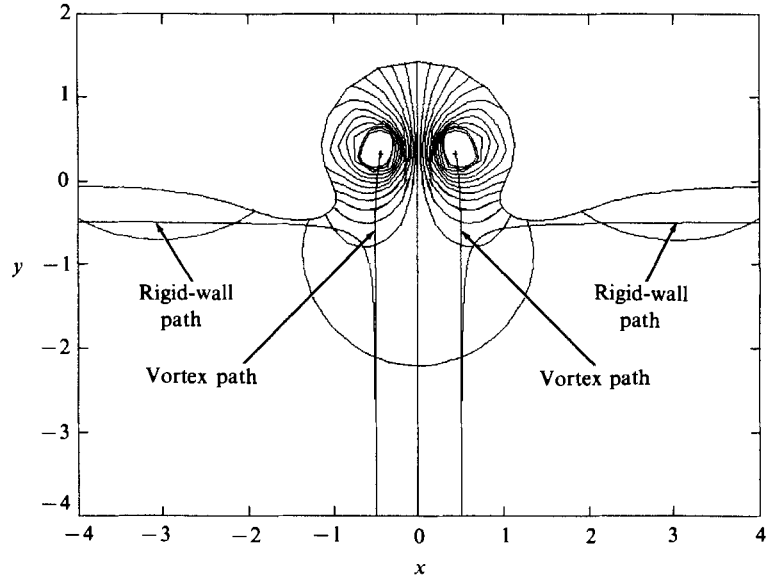

FIGURE 4. Streamlines $\psi = 0, \pm 0.02, \pm 0.04, \ldots, \pm 0.24$, vortex paths, wall paths, and the free surface for $1/F_r^2 = 0.02$ at $t = 34.0$.

Case (*b*) ($1/F_r^2 = 0.2$). For this case of intermediate circulation, the time step was initially chosen to be 0.25 and was kept at this value until $t = 20.0$, after which it was reduced several times until it was set to its final value of 0.003 for $t > 32.0$. Filtering of the free surface was also done only sparingly in this case. In particular, no filtering was used until t was greater than 20.0. For larger values of t the frequency of filtering varied from once for every five time steps to once per time step. The free surface, streamlines under the free surface, the position of the vortex pair and vortex paths

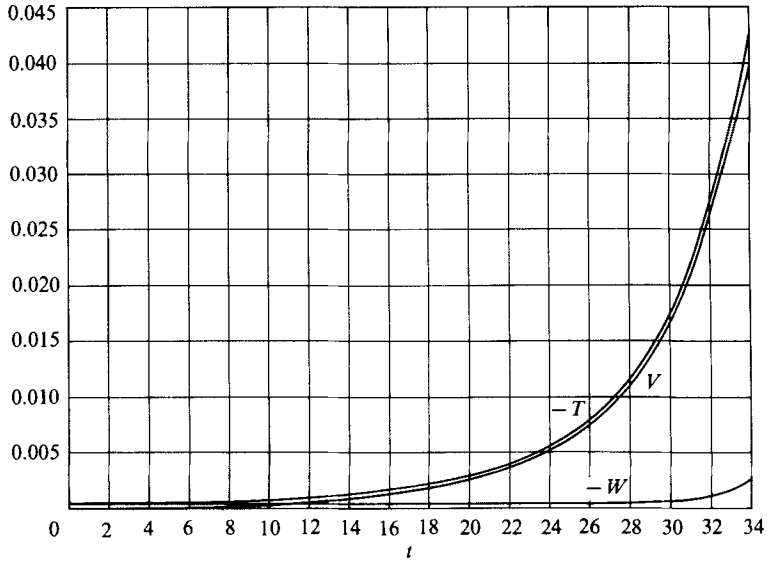

FIGURE 5. Potential energy (V), negative of 'finite' kinetic energy ($-T$), and negative of 'finite' total energy ($-W$) in the fluid versus time for $1/F_r^2 = 0.02$.

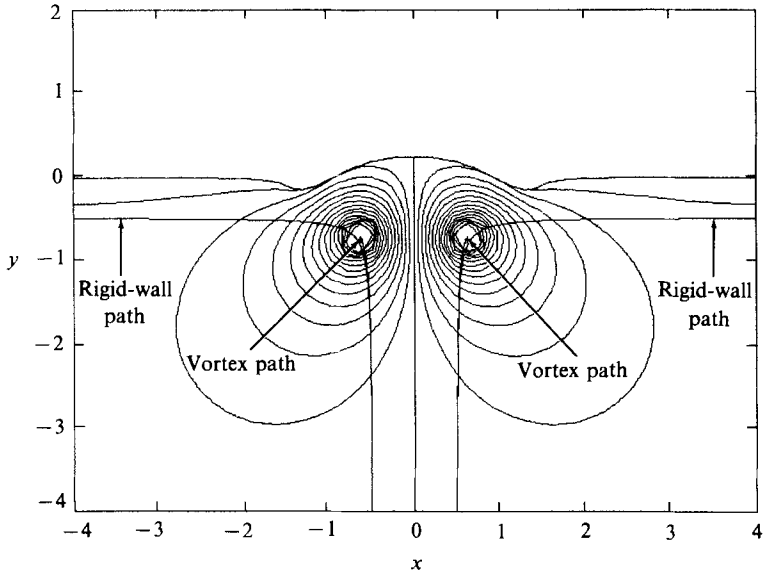

FIGURE 6. Streamlines $\psi = 0, \pm 0.02, \pm 0.04, \ldots, \pm 0.30$, vortex paths, wall paths, and the free surface for $1/F_r^2 = 0.2$ at $t = 30.0$.

are depicted in figures 6–10 for a sequence of five times near the end of the calculation. In this case the central hump in the free surface is much smaller than for $1/F_r^2 = 0.02$ while troughs form above the vortices and move out ahead of them. For $t > 33$ (figures 9 and 10), the curvature of the free surface in the troughs is so high that the computation could not be continued without a great loss in accuracy. Wave breaking is imminent and the limit of the validity of the irrotational flow model has been reached. The vortex paths are very close to the vortex paths for the rigid-wall

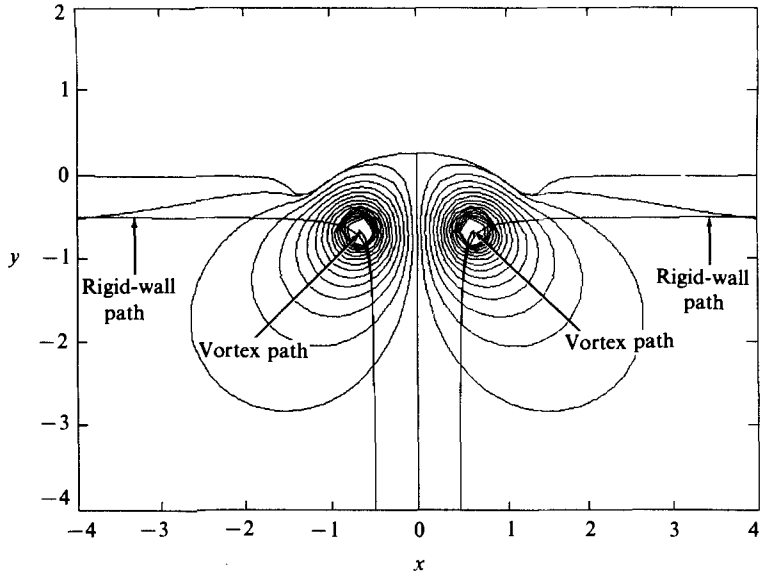

FIGURE 7. Streamlines $\psi = 0, \pm 0.02, \pm 0.04, \ldots, \pm 0.30$, vortex paths, wall paths, and the free surface for $1/F_r^2 = 0.2$ at $t = 31.0$.

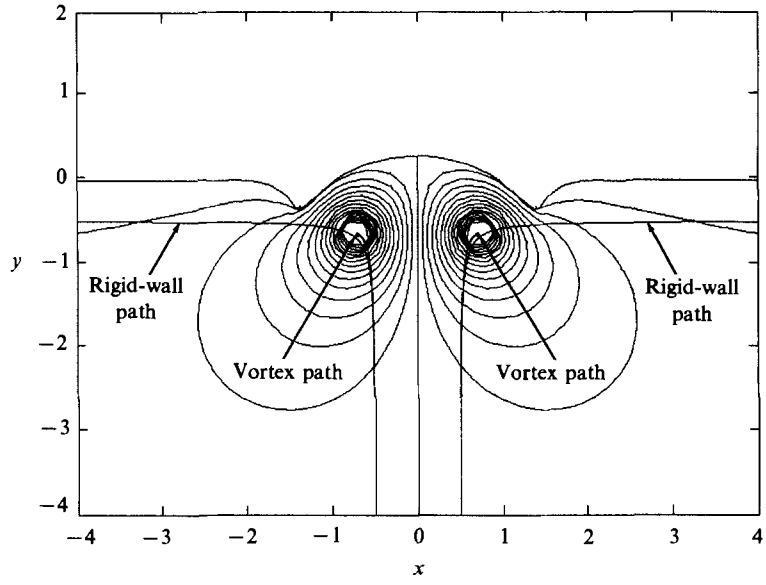

FIGURE 8. Streamlines $\psi = 0, \pm 0.02, \pm 0.04, \ldots, \pm 0.30$, vortex paths, wall paths, and the free surface for $1/F_r^2 = 0.2$ at $t = 32.0$.

case. In figure 10, which depicts the latest in the sequence of flow pictures, it appears that the paths of the vortices, after staying 'inside' the rigid-wall paths, are about to cross to the outside of these paths. The slight downward motion of the vortices is the result of the large free-surface slope near them and their tendency to move parallel to the boundary. The computed energy, kinetic energy and potential energy have been plotted in figure 11 as functions of time. As the calculation proceeds, the potential energy increases and is matched by a decrease in kinetic energy. Thus the

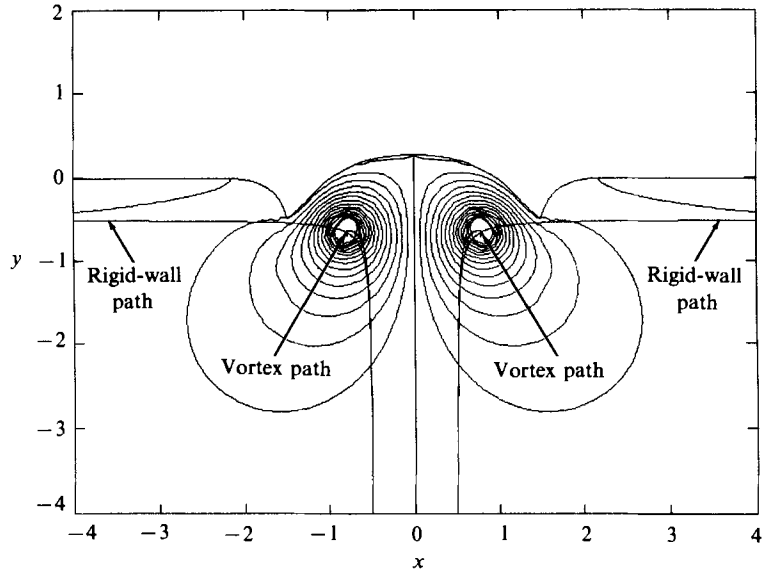

FIGURE 9. Streamlines $\psi = 0, \pm 0.02, \pm 0.04, \ldots, \pm 0.30$, vortex paths, wall paths, and the free surface for $1/F_\tau^2 = 0.2$ at $t = 33.08$.

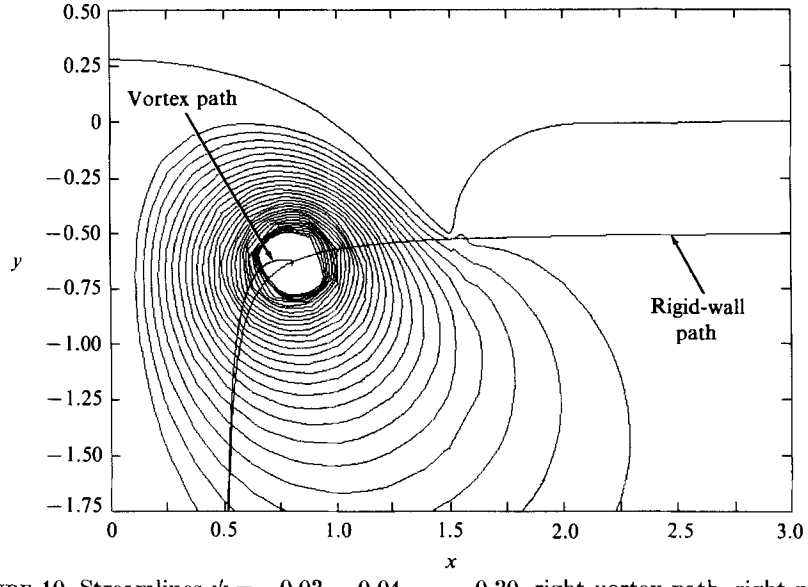

FIGURE 10. Streamlines $\psi = -0.03, -0.04, \ldots, -0.30$, right vortex path, right-wall path, and the free surface for $1/F_\tau^2 = 0.2$ at $t = 33.35$.

computed energy $-W$ is constant until the end of the calculation when $t > 32$. The decrease in kinetic energy is not inconsistent with the vortex paths crossing to the outside of the wall paths. The free-surface boundary is deformed so much that the simplified energy analysis for a straight boundary is no longer useful.

Case (c) ($1/F_\tau^2 = 4.0$). Figures 12–14 depict the vortex paths, streamlines and the free surface for three times near the end of the calculation. The time step used to obtain these results was 0.04 for $t < 20.0$, 0.01 for $20.0 < t < 31.0$, 0.005 for $31.0 < t < 32.0$ and 0.0025 for $t > 32.0$. Linear filtering was applied every two units

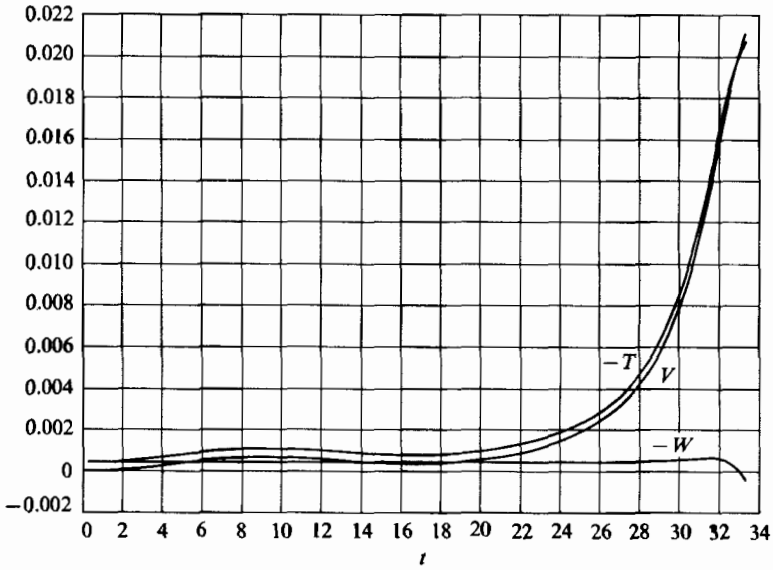

FIGURE 11. Potential energy (V), negative of 'finite' kinetic energy ($-T$), and negative of 'finite' total energy ($-W$) in the fluid versus time for $1/F_r^2 = 0.2$.

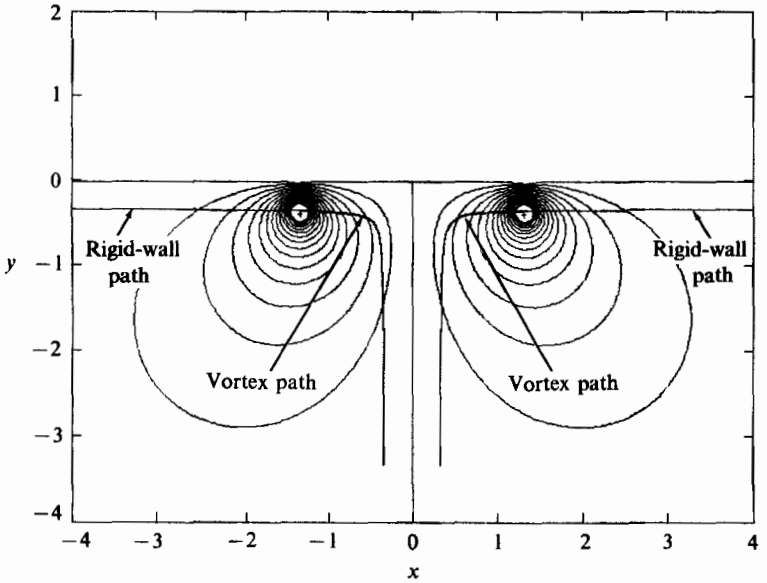

FIGURE 12. Streamlines $\psi = 0, \pm 0.02, \pm 0.04, \ldots, \pm 0.30$, vortex paths, wall paths, and the free surface for $1/F_r^2 = 4.0$ at $t = 41.75$.

of time until $t = 20.0$, then with increasing frequency until $t = 35.25$, and finally every 0.0025 units of time for $t > 35.25$, i.e. every time step. In this case the computed vortex paths are barely distinguishable from the vortex paths for the rigid-wall case. The shape of the free surface is not changed much by the presence of the vortices either.

If the reference frame is changed from a fixed one to one that moves with a point vortex, then the flow near the point vortex may be viewed as a nearly uniform steady

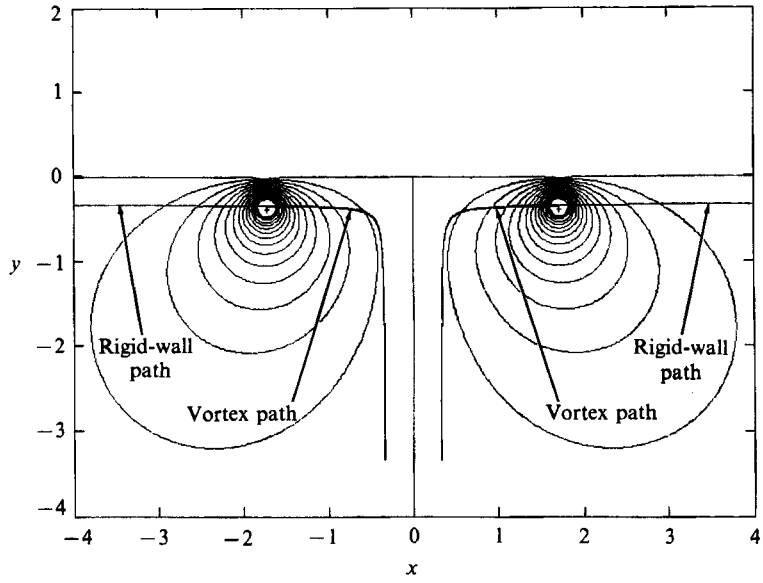

FIGURE 13. Streamlines $\psi = 0, \pm 0.02, \pm 0.04, \ldots, \pm 0.30$, vortex paths, wall paths, and the free surface for $1/F_r^2 = 4.0$ at $t = 45.75$.

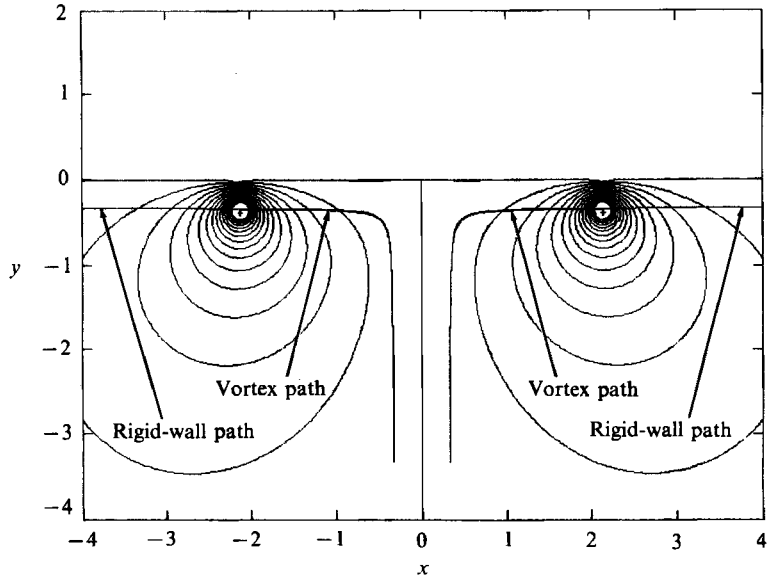

FIGURE 14. Streamlines $\psi = 0, \pm 0.02, \pm 0.04, \ldots, \pm 0.30$, vortex paths, wall paths, and the free surface for $1/F_r^2 = 4.0$ at $t = 49.75$.

stream flowing past it under the free surface. The fact that the flow near the discrete vortex is approaching a steady state in this reference frame is indicated in figure 15, where the free-surface elevations at four times, including the three previously plotted, are plotted with the vertical dimension enlarged by a factor of 56.25. The speed at which each vortex is moving horizontally is nearly equal to the speed with which it would move if the free surface were replaced with a rigid wall and its motion

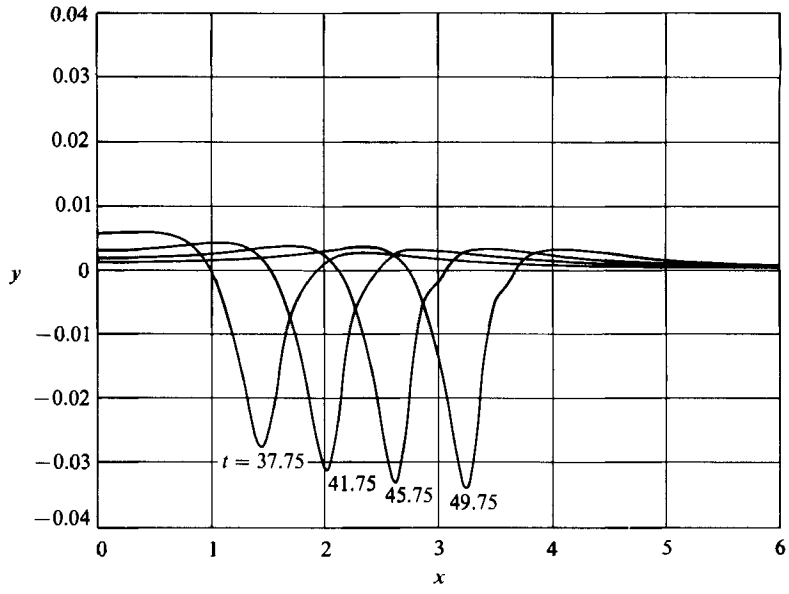

FIGURE 15. The computed free surface at $t = 37.75$, 41.75, 45.75 and 49.75 for $1/F_\tau^2 = 4.0$. The vertical scale is enlarged 56.25 times.

were induced entirely by the image system of a single reflected point vortex in the free surface.

For the vortex strength of this case, the corresponding linear solution of Novikov (1981) has a resonant steady-state wavetrain to one side of each of the discrete vortices. Its wavelength is $\pi\alpha$ and its amplitude is $4\pi e^{-1/\alpha}/\alpha$, where α is defined as $F_\tau^2/(2\pi^2)$. Thus the linear steady-state wavetrain resulting from each vortex has a wavelength of 0.04 and an amplitude of 5×10^{-32}, a vanishingly small number for practical purposes. In fact, the non-dimensional linear steady-state wave height $\eta(x)$ predicted by Novikov for a pair of vortices with one vortex of circulation -1 at $x_1-0.5i$ and the other of circulation 1 at $-x_1-0.5i$ is given by

$$\eta(x) = \frac{4\pi e^{-1/\alpha}}{\alpha}\left[H(x_1-x)\sin\frac{2(x-x_1)}{\alpha} - H(x+x_1)\sin\frac{2(x+x_1)}{\alpha}\right] + 2\alpha\int_0^\infty \frac{y(e^{-2|x-x_1|y}+e^{-2|x+x_1|y})(\cos y+\alpha y\sin y)}{1+\alpha^2y^2}\,dy. \quad (28)$$

Here $H(x)$ is 1 if x is positive and -1 if x is negative. Figure 16 shows a comparison of the computed nonlinear free surface at the time $t = 49.75$ with the free-surface elevation $\eta(x)$. The prediction of linear theory is for a somewhat broader and shallower depression than the depression predicted by the nonlinear calculations. However, the positions of the troughs are almost identical.

The plots of energy, kinetic energy and potential energy in figure 17 also indicate that the flow may be approaching a steady state since all three energy curves are approximately level for the latest computed times. The curve for $-W$ stays constant at about 4.0×10^{-4} until approximately $t = 35$ at which time it rises before it levels off again for $t > 40$. The rise in the curve indicates a loss of total energy in the fluid since the curve actually represents the negative of the finite part of the total energy

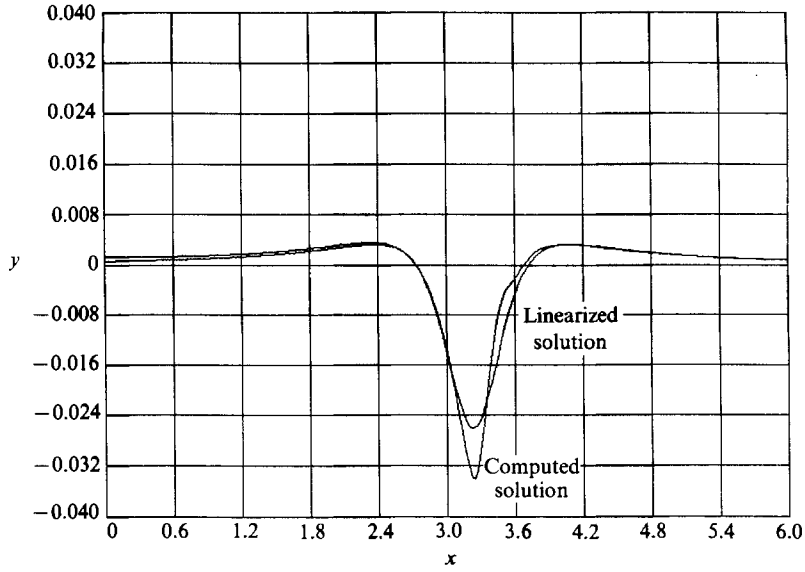

FIGURE 16. The computed free surface and the solution of a corresponding linearized free-surface flow problem at $t = 49.75$ for $1/F_\tau^2 = 4.0$.

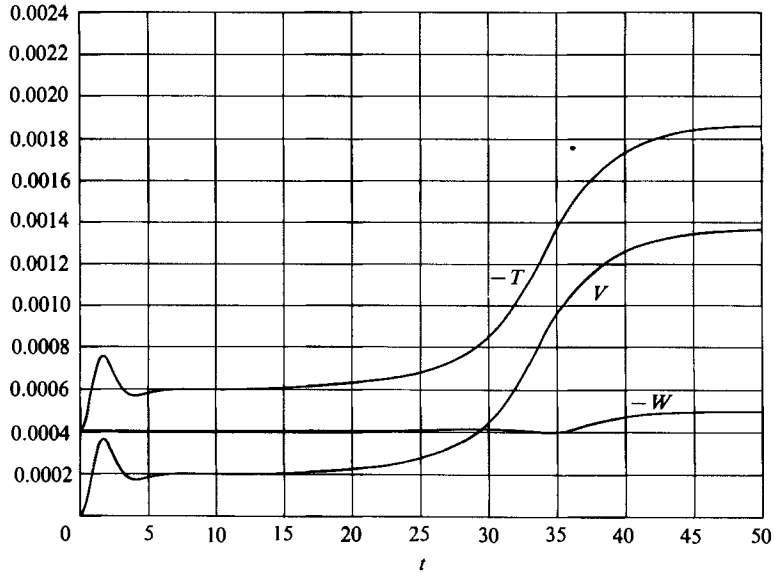

FIGURE 17. Potential energy (V), negative of 'finite' kinetic energy ($-T$), and negative of 'finite' total energy ($-W$) in the fluid versus time for $1/F_\tau^2 = 4.0$.

in the fluid. While the energy curve is rising, i.e. for $t > 35$, small waves, which were generated at the start ($t = 0$) and which travelled rapidly out from the origin, are being damped as they move into regions with ever larger mesh spacing. The loss of energy due to this damping accounts, at least partially, for the rise in the curve of $-W$ of figure 17.

5. Conclusion

The nonlinear free-surface potential-flow problem of a pair of counter-rotating point vortices approaching a free surface and interacting with it has been solved numerically for three ratios of circulation to initial separation. The solutions are thus new results that extend the solutions given by Lamb (1932) for a rigid wall. For large circulation it is found that the vortex pair rises rapidly, surpasses the height of the mean surface level and produces a large hump on the free surface after initially following the paths of the rigid-wall case. Free-surface breaking will occur. For an intermediate value of circulation, the vortices follow the rigid-wall paths more closely, but at the time the rigid-wall vortices turn to move outward instead of upward, the curvature of the free surface above the point vortices becomes so high that the calculation had to be terminated. Breaking again occurs. For weak circulation the vortices follow the paths of the rigid-wall case closely. The energy and the free-surface elevation suggest that the flow may approach a steady state for weak circulation. A steady state is, of course, theoretically impossible because energy must continually be converted from kinetic to potential to maintain the wavetrain that would develop. However, since the amplitude of the wavetrain is extremely small in the case of weak circulation, an essentially steady-state solution has been computed and that solution is very close to the rigid-wall solution.

In the light of these results, it seems unlikely that a significant wavetrain behind an isolated vortex moving parallel to the water surface can occur when that vortex starts out as one of a pair moving vertically towards the surface. Either the vortex will be too weak to generate such a wavetrain, or, if it is stronger, the original pair will induce wave breaking and the vortices will not smoothly turn the corner to move apart parallel to the surface.

For each of the cases, the finite part of the total energy in the fluid has been calculated and has been found to be nearly constant except near the end of the calculations when the spacing of the points on the free surface has become quite coarse.

This work was supported by the Numerical Naval Hydrodynamics Program at the David Taylor Research Center. This program is sponsored jointly by the DTRC Independent Research Program and the Office of Naval Research.

Appendix. Energy conservation

If the potential energy V, non-dimensionalized by $\rho\Gamma^2$, is initially defined to be zero, it may be calculated at any time from the free-surface integral

$$V = \frac{1}{2F_r^2}\int_{-\infty}^{\infty} y^2 n_y \, \mathrm{d}s. \tag{A 1}$$

The kinetic energy, on the other hand, is always infinite because of the singular nature of the vortices, and its treatment here is based on the treatment used by Batchelor (1967) to obtain an integral invariant for the motion of a group of point vortices in an unbounded fluid domain. The difference is that here the fluid is bounded by a free surface, rather than filling the entire two-dimensional plane. Consider the portion of the fluid domain bounded by the free surface, a circle of radius ϵ about each point vortex, and a semicircle of large radius R about the origin.

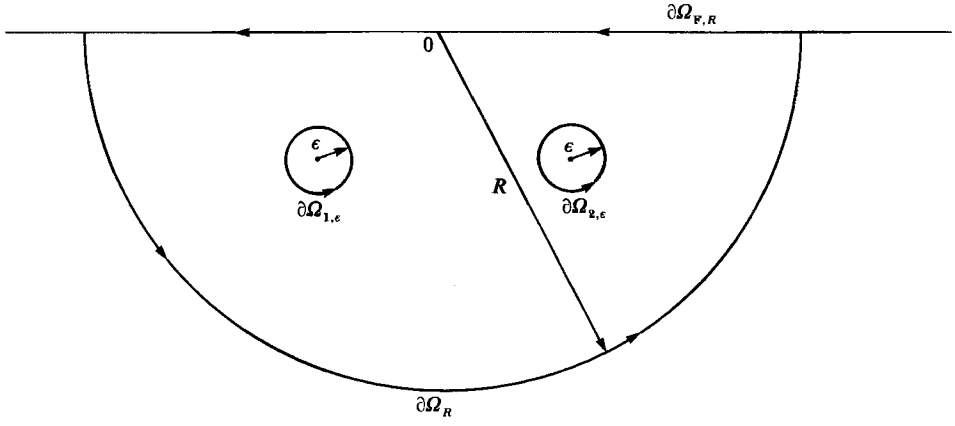

FIGURE 18. Integration paths for equation (A 2).

Denote this region by $\Omega_{R,\epsilon}$, its free-surface boundary by $\partial\Omega_{F,R}$, the outer semi-circular arc by $\partial\Omega_R$, the circular path about the first vortex by $\partial\Omega_{1,\epsilon}$ and the circular path about the second vortex by $\partial\Omega_{2,\epsilon}$. According to Batchelor, the total kinetic energy of the fluid contained in the region $\Omega_{R,\epsilon}$ is given by the formula

$$\begin{aligned} T_{R,\epsilon} &= -\frac{1}{2}\int_{\partial\Omega} \psi \boldsymbol{v}\cdot \mathrm{d}\boldsymbol{x} \\ &= -\frac{1}{2}\int_{\partial\Omega_R} \psi \boldsymbol{v}\cdot \mathrm{d}\boldsymbol{x} - \frac{1}{2}\int_{\partial\Omega_{F,R}} \psi \boldsymbol{v}\cdot \mathrm{d}\boldsymbol{x} + \frac{1}{2}\int_{\partial\Omega_{1,\epsilon}} \psi \boldsymbol{v}\cdot \mathrm{d}\boldsymbol{x} + \frac{1}{2}\int_{\partial\Omega_{2,\epsilon}} \psi \boldsymbol{v}\cdot \mathrm{d}\boldsymbol{x}, \end{aligned} \quad (A\,2)$$

where ψ denotes the stream function and $\boldsymbol{v}$ denotes the fluid velocity. The paths of integration are traversed in the directions indicated in figure 18. The stream function is written as

$$\psi(x,y) = \psi_0(x,y) - \frac{1}{4\pi}\log\{(x-x_1)^2+(y-y_1)^2\} + \frac{1}{4\pi}\log\{(x-x_2)^2+(y-y_2)^2\}$$

for (x,y) not at a discrete vortex, in which for free-surface flow the function $\psi_0(x,y)$ is defined to be

$$\psi_0(x,y) = -\frac{1}{4\pi}\int_{-\infty}^{\infty} \gamma(e')\log\{(x-x_F(e'))^2+(y-y_F(e'))^2\}\,\mathrm{d}e'.$$

On the paths $\partial\Omega_{j,\epsilon}$, for $j = 1, 2$, the asymptotic behaviour, for $\epsilon \to 0$, of the stream function ψ is given by

$$\psi(x,y) \sim \psi_0(x_j,y_j) - \frac{(-1)^j}{2\pi}\log r_{12} + \frac{(-1)^j}{2\pi}\log\epsilon,$$

where r_{12} is the distance between the two discrete vortices. It is the log-ϵ term that leads to infinite kinetic energy. On the path $\partial\Omega_R$, the asymptotic behaviour, for $R \to \infty$, of ψ is not immediately apparent. However, one can consider the corresponding linearized free-surface potential-flow problem for a pair of point vortices brought into existence at $t = 0$. Even if the conditions for linearizing the problem are not satisfied on the free surface near the point vortices, the flow at a large distance from the two point vortices is approximated well by the linear solution during the finite interval of time for which calculations are performed. Using the solution of

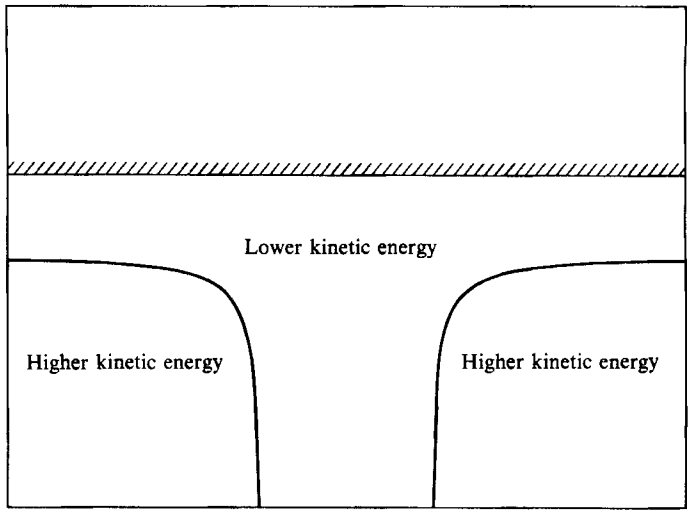

FIGURE 19. Constant-kinetic-energy paths for a pair of vortices approaching a rigid wall, according to Lamb (1932).

Wehausen & Laitone (1960) for a single vortex, one can write the solution of the linearized problem as

$$\begin{aligned} w(z,t) &= \phi(x,y)+\mathrm{i}\psi(x,y) \\ &= \frac{1}{2\pi\mathrm{i}}\log(z-z_1(t))-\frac{1}{2\pi\mathrm{i}}\log(z-z_2(t))+\frac{1}{2\pi\mathrm{i}}\log(z-z_1^*(t))-\frac{1}{2\pi\mathrm{i}}\log(z-z_2^*(t)) \\ &\quad +\frac{1}{\pi\mathrm{i}}\int_0^t \mathrm{d}\tau\int_0^\infty \frac{1}{k^{\frac{1}{2}}}\exp[-\mathrm{i}F_r^2 k(z-z_1^*(\tau))]\sin[k^{\frac{1}{2}}(t-\tau)]\,\mathrm{d}k \\ &\quad -\frac{1}{\pi\mathrm{i}}\int_0^t \mathrm{d}\tau\int_0^\infty \frac{1}{k^{\frac{1}{2}}}\exp[-\mathrm{i}F_r^2 k(z-z_2^*(\tau))]\sin[k^{\frac{1}{2}}(t-\tau)]\,\mathrm{d}k, \end{aligned}$$

where all variables are non-dimensional. Since the inner integrals in the last two terms are $O(1/R)$ for $R\to\infty$, as has been shown for similar integrals by Lamb (1932), the stream function $\psi(x,y)$ vanishes at least as fast as $1/R$ as $R\to\infty$. Thus the integral over the outer semicircle for the kinetic energy vanishes as R approaches infinity. Letting $\epsilon\to 0$ and $R\to\infty$ in (A 2), one obtains

$$T=\lim_{\epsilon\to 0,\ R\to\infty}\left(T_{R,\epsilon}+\frac{1}{2\pi}\log\epsilon\right)=\psi_0(x_1,y_1)+\frac{1}{2}\int_{-\infty}^{\infty}\psi\boldsymbol{v}\cdot\mathrm{d}\boldsymbol{x}+\frac{1}{2\pi}\log r_{12}. \qquad (A\ 3)$$

The quantity T, which is obtained by removing the log-ϵ term from the kinetic energy, is called the finite part of the kinetic energy. It is conjectured that

$$W=V+T \qquad (A\ 4)$$

is invariant.

For the case of a rigid wall replacing the free surface, the function $\psi_0(x,y)$ represents the image system for the two vortices given by

$$\psi_0(x,y)=\frac{1}{4\pi}\log\{(x-x_1)^2+(y+y_1)^2\}-\frac{1}{4\pi}\log\{(x-x_2)^2+(y+y_2)^2\}.$$

In this case, the integral over $\partial\Omega_{\mathrm{F},R}$ in (A 2) vanishes since the boundary $\partial\Omega_{\mathrm{F},R}$ is a flat surface on which ψ vanishes. Moreover, it is easy to see that the integral over $\partial\Omega_R$ vanishes as $R\to\infty$. Thus,

$$T=\lim_{\epsilon\to 0,\ R\to\infty}\left(T_{R,\epsilon}+\frac{1}{2\pi}\log\epsilon\right)=\frac{1}{4\pi}\log\left\{\frac{4x_1^2y_1^2}{x_1^2+y_1^2}\right\}. \tag{A 5}$$

It can be seen from (A 5) that T = constant is the equation for the paths of Lamb's (1932) solution for the vortices approaching a wall (figure 19). Thus the conjecture that $V+T$ is invariant is verified at least for this special case when $V\equiv 0$. Moreover, T is a monotonically increasing function of the square of the initial separation between the vortices. Thus a deviation of the vortices from the paths of the wall solution represents an increase in kinetic energy if the new paths lie 'outside' the constant-T paths as indicated in figure 19. Otherwise the new paths represent a decrease in kinetic energy.

With the free surface in place of the wall, some of the kinetic energy will be converted to potential energy. The reduction in kinetic energy would tend to lead to vortex paths that are 'inside' the wall paths. However, the deformation of the upper boundary will further distort the paths so that energy analysis alone is inadequate for predicting the paths in the free-surface case.

REFERENCES

Baker, G. R., Meiron, D. I. & Orszag, S. A. 1981 Applications of a generalized vortex method to nonlinear free surface flows. *Proc. Third Intl Conf. on Numerical Ship Hydrodynamics, Paris.*

Baker, G. R., Meiron, D. I. & Orszag, S. A. 1982 Generalized vortex methods for free-surface flow problems. *J. Fluid Mech.* **123**, 477–501.

Barker, S. J. & Crow, S. C. 1977 The motion of two-dimensional vortex pairs in a ground effect. *J. Fluid Mech.* **82**, 659–671.

Batchelor, G. K. 1967 *An Introduction to Fluid Dynamics.* Cambridge Univerity Press.

Haussling, H. J. & Coleman, R. M. 1979 Nonlinear water waves generated by an accelerated circular cylinder. *J. Fluid Mech.* **92**, 767–781.

Israeli, M. & Orszag, S. A. 1981 Approximation of radiation boundary conditions. *J. Comput. Phys.* **41**, 115–135.

Lamb, H. 1932 *Hydrodynamics.* Dover.

Longuet-Higgins, M. S. & Cokelet, E. D. 1976 The deformation of steep surface waves. I. A numerical method of computation. *Proc. R. Soc. Lond.* A **350**, 1–26.

Novikov, Y. A. 1981 Generation of surface waves by discrete vortices. *Izv., Atmospheric and Oceanic Phys.* **17**, 709–714.

Peace, A. J. & Riley, N. 1983 A viscous vortex pair in ground effect. *J. Fluid Mech.* **129**, 409–426.

Saffman, P. G. 1979 The approach of a vortex pair to a plane surface in inviscid fluid. *J. Fluid Mech.* **92**, 497–503.

Salvesen, N. & von Kerczek, C. 1976 Comparison of numerical and perturbation solutions of two-dimensional nonlinear water-wave problems. *J. Ship Res.* **20**, 160–170.

Sarpkaya, T. & Henderson, D. O. 1984 Surface disturbances due to trailing vortices. *Naval Postgraduate School Rep. NPS*-69-84-004, Monterey, California.

Shapiro, R. 1975 Linear filtering. *Math. Comp.* **29**, 1094–1097.

Wehausen, J. V. & Laitone, E. V. 1960 Surface waves. In *Encyclopedia of Physics*, vol. IX, pp. 446–778. Springer.